Six6 and Six7 coordinately regulate expression of middle-wavelength opsins in zebrafish

Yohey Ogawa[a], Tomoya Shiraki[a,b], Yoshimasa Asano[a], Akira Muto[b,c], Koichi Kawakami[b,c], Yutaka Suzuki[d], Daisuke Kojima[a,1], and Yoshitaka Fukada[a,1]

[a]Department of Biological Sciences, School of Science, The University of Tokyo, 113-0033 Tokyo, Japan; [b]Laboratory of Molecular and Developmental Biology, National Institute of Genetics, Mishima, 411-8540 Shizuoka, Japan; [c]Department of Genetics, SOKENDAI (The Graduate University for Advanced Studies), Mishima, 411-8540 Shizuoka, Japan; and [d]Graduate School of Frontier Sciences, The University of Tokyo, Kashiwa, 277-0882 Chiba, Japan

Edited by Pamela A. Raymond, University of Michigan, Ann Arbor, MI, and accepted by Editorial Board Member Jeremy Nathans January 11, 2019 (received for review July 26, 2018)

Color discrimination in the vertebrate retina is mediated by a combination of spectrally distinct cone photoreceptors, each expressing one of multiple cone opsins. The opsin genes diverged early in vertebrate evolution into four classes maximally sensitive to varying wavelengths of light: UV (SWS1), blue (SWS2), green (RH2), and red (LWS) opsins. Although the tetrachromatic cone system is retained in most nonmammalian vertebrate lineages, the transcriptional mechanism underlying gene expression of the cone opsins remains elusive, particularly for SWS2 and RH2 opsins, both of which have been lost in the mammalian lineage. In zebrafish, which have all four cone subtypes, *rh2* opsin gene expression depends on a homeobox transcription factor, *sine oculis* homeobox 7 (Six7). However, the *six7* gene is found only in the ray-finned fish lineage, suggesting the existence of another evolutionarily conserved transcriptional factor(s) controlling *rh2* opsin expression in vertebrates. Here, we found that the reduced *rh2* expression caused by *six7* deficiency was rescued by forced expression of *six6b*, which is a *six7*-related transcription factor conserved widely among vertebrates. The compensatory role of *six6b* was reinforced by ChIP-sequencing analysis, which revealed a similar pattern of Six6b- and Six7-binding sites within and near the cone opsin genes. TAL effector nuclease-induced genetic ablation of *six6b* and *six7* revealed that they coordinately regulate SWS2 opsin gene expression. Mutant larvae deficient for these transcription factors showed severely impaired visually driven foraging behavior. These results demonstrate that in zebrafish, *six6b* and *six7* govern expression of the SWS2 and RH2 opsins responsible for middle-wavelength sensitivity, which would be physiologically important for daylight vision.

photoreceptor development | transcription factor | cone opsin | zebrafish retina | color vision

In vertebrates, vision is triggered by light stimulation of two structurally and functionally distinct retinal photoreceptor cell types: rods and cones (1, 2). Cones function under daylight conditions, and color discrimination is conferred by a combination of spectrally distinct cone subtypes, each of which expresses a specific visual pigment (cone opsin). Cone opsin genes are subdivided into four classes: UV [short wavelength-sensitive 1 (SWS1), wavelength of maximum sensitivity (λ_{max}): 360–420 nm], blue [short wavelength-sensitive 2 (SWS2), λ_{max}: 400–470 nm], green [middle wavelength-sensitive (RH2), λ_{max}: 460–510 nm], and red [long wavelength-sensitive (LWS), λ_{max}: 510–560 nm] opsin genes (3, 4). These four classes are thought to have emerged early in vertebrate evolution because they are found in the genome of the pouched lamprey (3, 5) (Fig. 1), a jawless vertebrate whose ancestor diverged from a lineage leading to jawed vertebrates more than 500 Mya. The four cone subtypes have been retained in a substantial number of vertebrate clades, such as fish, reptiles, and birds (6, 7), suggesting that tetrachromatic color discrimination is evolutionarily advantageous.

Cone subtypes are defined by the cone opsin genes they express. A number of studies have reported key transcription factors responsible for expression of the cone opsin genes in vertebrates (8, 9). Cone-rod homeobox (*crx*) is a master transcriptional regulator for development of rod and cone photoreceptors (10, 11). Thyroid hormone receptor beta (*thrb*) is essential for LWS opsin gene expression (12, 13). These studies on the transcriptional regulation of the opsin genes have been mainly performed in mice, which have only three types of photoreceptor: rods and two cone subtypes, SWS1 and LWS cones. To understand transcriptional mechanisms underlying the tetrachromatic cone system, the zebrafish is a valuable animal model in that it has all four cone subtypes. The zebrafish has been used for revealing retinal development (14, 15). Genetic analysis in zebrafish showed that T-box 2b (*tbx2b*) is necessary for *sws1* opsin gene expression (16). We have recently found that *sine oculis* homeobox 7 (*six7*), present only in the ray-finned fish lineage, is required for *rh2* opsin gene expression (17). Intriguingly, *rh2* opsin genes are widely present in vertebrate lineages (Fig. 1), suggesting the existence of another evolutionarily conserved transcriptional factor(s) responsible for *rh2* opsin gene expression in vertebrates. Another missing regulator is a transcription factor essential for *sws2* opsin expression, since deletion of *six7* reduced *sws2* opsin mRNA only by half (17).

Significance

Color discrimination in the vertebrate retina is mediated by a combination of cone cell types expressing UV (SWS1), blue (SWS2), green (RH2), and red (LWS) opsins. Although the tetrachromatic cone system is retained in most nonmammalian vertebrate lineages, the transcriptional mechanism underlying gene expression of cone opsins remains elusive. Here, we found that the retinal transcription factors, *sine oculis* homeobox 6 (Six6b) and Six7, synergistically and positively regulate gene expression of zebrafish SWS2 and RH2 opsins. Larvae deficient for both of these transcription factors showed heavily impaired visually driven foraging behavior and were unable to compete for food when reared in a group with normal siblings. The results suggest that *six6b* and *six7* play a pivotal role in blue- and green-light sensitivity and daylight vision.

Author contributions: Y.O., T.S., D.K., and Y.F. designed research; Y.O., T.S., A.M., K.K., Y.S., and D.K. performed research; Y.O. and Y.A. analyzed data; and Y.O., D.K., and Y.F. wrote the paper.

The authors declare no conflict of interest.

This article is a PNAS Direct Submission. P.A.R. is a guest editor invited by the Editorial Board.

Data deposition: The ChIP-sequencing data reported in this paper have been deposited in the DNA Bank of Japan (DDBJ; https://www.ddbj.nig.ac.jp/index-e.html), European Molecular Biology Laboratory (EMBL), and National Center for Biotechnology Information (NCBI) databases (https://www.ncbi.nlm.nih.gov/bioproject) (accession no. PRJDB7218). The plasmid sequences reported in this paper have been deposited in the DDBJ, EMBL, and NCBI databases [accession nos. LC413281 (Six7) and LC413282 (Six6b)].

[1]To whom correspondence may be addressed. Email: sdkojima@mail.ecc.u-tokyo.ac.jp or sfukada@mail.ecc.u-tokyo.ac.jp.

This article contains supporting information online at www.pnas.org/lookup/suppl/doi:10.1073/pnas.1812884116/-/DCSupplemental.

Published online February 14, 2019.

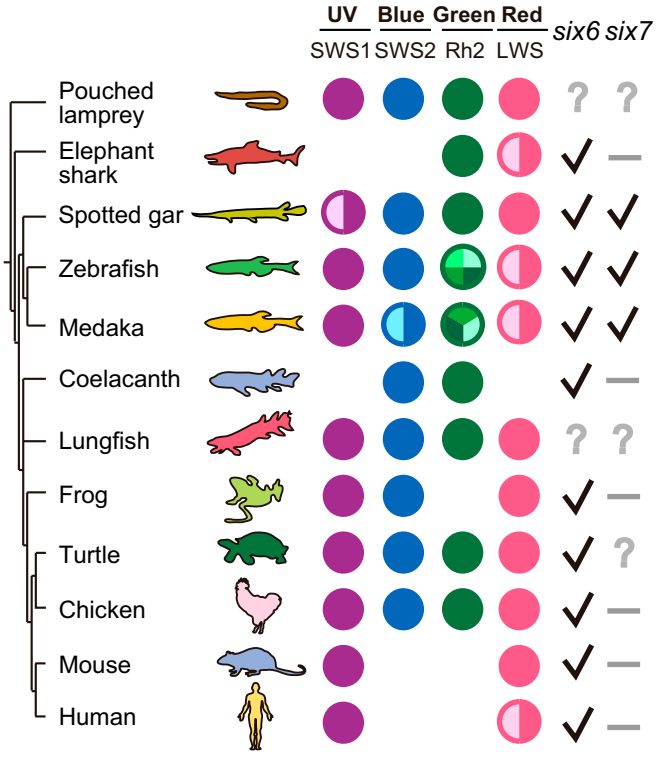

Fig. 1. Presence of cone opsin classes and *sine oculis* transcription factors, *six6* and *six7*, within representative vertebrate clades. The presence (circle) or absence (blank) of each class of cone opsin gene is presented according to previous studies (6, 33). In each circle, the number of colored partitions indicates the number of duplicated gene(s). The presence (checkmark) or absence (minus sign) of *six6* gene is indicated, and the accession numbers are listed in *SI Appendix*, Table S1. Similarly, the presence or absence of the *six7* gene is presented according to our previous study (17). Pouched lamprey, *Geotria australis*; Elephant shark, *Callorhinchus milii*; Spotted gar, *Lepisosteus oculatus*; Zebrafish, *Danio rerio*; Medaka, *Oryzias latipes*; Coelacanth, *Latimeria chalumnae*; Lungfish, *Neoceratodus forsteri*; Frog, *Xenopus tropicalis*; Turtle, *Pelodiscus sinensis*; Chicken, *Gallus gallus*; Mouse, *Mus musculus*; Human, *Homo sapiens*.

In the present study, we investigated the roles of *six7*-related transcription factors, *six6a* and *six6b*, in the control of *sws2* and *rh2* opsin expression in zebrafish. We found that *six6b* has functional similarity to *six7* in regulating *rh2* opsin gene expression, and demonstrated that triple knockout (TKO) of *six6a*, *six6b*, and *six7* completely abolished not only *rh2* but also *sws2* opsin expression. In addition, the TKO larvae exhibited severely impaired foraging behavior. We demonstrate that complementary regulation by *six6* and *six7* is indispensable for expression of middle wavelength-sensitive blue (SWS2) and green (RH2) opsin genes, which are important for daylight vision.

Results

Expression of *six6a* and *six6b* in Zebrafish Retina. Members of the *sine oculis* (Six) family of homeodomain transcription factors play important roles in vertebrate eye development (18). The Six7 subfamily, conserved only in the ray-finned fishes, diverged before the split between Six3 and Six6 subfamilies (Fig. 2*A*), which are widely conserved among vertebrate species. The zebrafish genome contains two members of the *six3* subfamily (*six3a* and *six3b*) and two members of the *six6* subfamily (*six6a* and *six6b*), which are likely to have arisen via teleost-specific whole-genome duplication (19). Among these paralogous genes, only *six6a* and *six6b* were enriched in cones (Fig. 2*B* and *SI Appendix*, Fig. S1). Both *six6a* and *six6b* were expressed predominantly in the eyes at both the larval and adult stages (Fig. 2*C*). Whole-mount in situ hybridization in the larvae detected expression of *six6b* in the eye and a region of the brain (Fig. 2*D*). Further analysis using larval and adult eye sections revealed *six6b* expression in the photoreceptor layer, as well as in the retinal ganglion cells and the inner half of the inner nuclear layer (Fig. 2 *E* and *F*). In the photoreceptor layer, *six6b*-positive nuclei were mainly located in the cone nuclear layer (Fig. 2*F*), consistent with the cone-enriched expression profile of *six6b* in isolated photoreceptors (Fig. 2*B* and *SI Appendix*, Fig. S1). In the larval retina, *six6b* expression was also detected in the ciliary marginal zone of the peripheral retina (Fig. 2*E*), where proliferating cells reside (20). In contrast, retinal *six6a* expression was undetectable by in situ hybridization. Consistently, the expression level of *six6a* was about ninefold lower than that of *six6b* in a previous RNA-sequencing analysis of larval zebrafish retina (21). These data suggest that *six6b* predominantly contributes to cone photoreceptor development and/or function.

Functional Compensation of *six7* Deficiency by Six6b. The conservation of the *six7* gene only in ray-finned fishes, together with the cone-enriched expression of both *six6b* and *six7* (17) (Fig. 2*B*), suggests that *six6b* may play a role in regulating green (*rh2*) opsin gene expression in vertebrate species other than ray-finned fish. We asked whether forced expression of *six6b* in photoreceptors rescues the phenotypes caused by *six7* KO, in which expression of all of the four *rh2* genes (*rh2-1*, *rh2-2*, *rh2-3*, and *rh2-4*) is severely reduced (17). For this purpose, we generated two lines (ja70Tg and ja73Tg) of *six6b* transgenic zebrafish (hereafter referred to as *six6b-tg*), which were designed to express both EGFP and FLAG-tagged Six6b from a single ORF by using a viral 2A peptide under the control of *crx* promoter (Fig. 3*A*). The *crx* promoter drives gene expression in developing and differentiated photoreceptors (12). In the transgenic fish, all types of photoreceptors were found to express EGFP (Fig. 3 *B* and *C* and *SI Appendix*, Fig. S2*A*). In the 5-d postfertilization (dpf) larvae, we examined mRNA levels of all of the rod and cone opsins, among which those of *lws1*, *rh2-3*, and *rh2-4* are known to be extremely low (22). The deficiency of *six7* greatly decreased the expression levels of blue (*sws2*), *rh2-1*, and *rh2-2* opsin mRNA and increased the expression levels of red (*lws1* and *lws2*) opsin mRNA (Fig. 3*D*). The reduced mRNA levels of *rh2-1* and *rh2-2* were partially but significantly restored when *six6b-tg* (ja70Tg) was introduced into *six7* KO mutant (*six6b-tg;six7* KO; Fig. 3*D* and *SI Appendix*, Fig. S2*B*). Similarly, reduced expression of *sws2* opsin mRNA and enhanced expression of *lws1* and *lws2* opsin mRNA in *six7* KO were both restored to levels close to those of wild type (WT; Fig. 3*D* and *SI Appendix*, Fig. S2*B*). The extremely low levels of *rh2-3* and *rh2-4* mRNAs (22) were not affected by *six6b* overexpression (*SI Appendix*, Fig. S2*B*). On the other hand, forced expression of *six6b* in the WT background caused no marked change in mRNA levels of rod and cone opsins (Fig. 3*E* and *SI Appendix*, Fig. S2*C*). The restoration of *sws2* and *rh2* opsin mRNA expression in *six6b-tg;six7* KO mutant retina was confirmed by in situ hybridization (Fig. 3 *F* and *G*). All of these phenotypes were also observed when the second *six6b-tg* line (ja73Tg) was used (*SI Appendix*, Fig. S3), supporting the conclusion that *six6b* functionally compensates for the *six7* deficiency. These results demonstrate that *six6b* is capable of regulating gene expression of *sws2*, *rh2*, and *lws* cone opsins in the absence of *six7*.

Similarities in Binding Motifs and Target Genes Between Six6b and Six7. To investigate whether Six6b and Six7 share target genes, we employed ChIP sequencing (ChIP-seq) to identify their binding sites across the genome. We used an anti-FLAG antibody to immunoprecipitate chromatin from the retinas of adult transgenic fish, *six6b-tg* (ja70Tg) or *six7-tg* (ja69Tg), in which FLAG-tagged Six6b or Six7 protein was expressed, respectively, in photoreceptor cells under the control of the *crx* promoter (12) (*SI Appendix*, Fig. S4). In both *six6b-tg* and *six7-tg* retinas, enrichment of the ChIP-seq signal was observed in the promoter region of blue opsin gene, *sws2* (23) (Fig. 4*A*, *Upper*), and in the promoter and enhancer regions of green opsin genes, *rh2-1, rh2-2,*

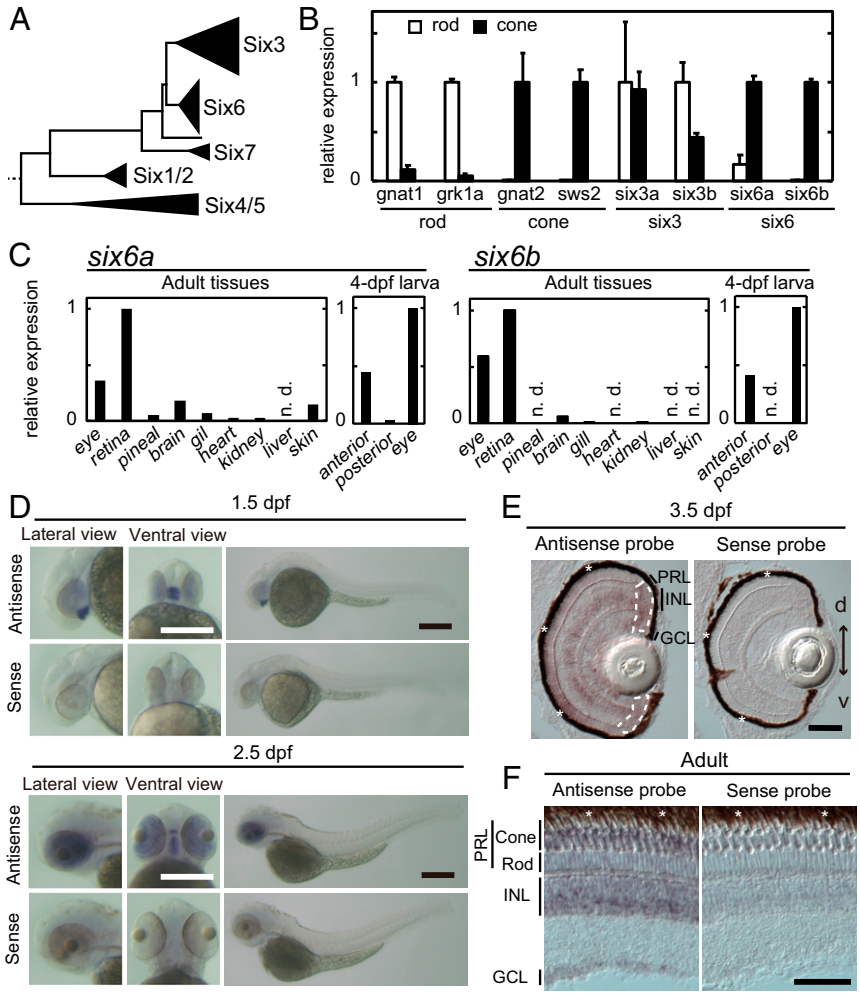

Fig. 2. Expression pattern of *six6a* and *six6b*. (*A*) Schematic representation of the phylogenetic tree of the Six family, modified from our previous study (17). Relative expression levels of *six6a* and *six6b* are shown in isolated rods and cones at the adult stage (mean ± SD, $n = 2$) (*B*) and in adult and 4-dpf larval tissues (*C*). *n.d.*, not detected. Photoreceptor purity after isolation was further validated in *SI Appendix*, Fig. S1. Expression patterns of *six6b* examined by in situ hybridization in whole-mount embryos at 1.5 dpf and 2.5 dpf (*D*), in the larval retina at 3.5 dpf (*E*), and in the 6-mo postfertilization adult retina (*F*) are shown. In *E*, ciliary marginal zones are surrounded by white broken lines. d, dorsal side; GCL, ganglion cell layer; INL, inner nuclear layer; PRL, photoreceptor layer; v, ventral side. The retinal pigmented epithelium (indicated by asterisks) is adjacent to the photoreceptor layer. (Scale bars: *D*, 300 μm; *E* and *F*, 50 μm.)

rh2-3, and *rh2-4* (24) (Fig. 4*A*, *Lower*). Enrichment in these seven regions was validated by ChIP-qPCR (Fig. 4*B*). Two of the seven regions, region 1 in *sws2* (23) and region 3 in *rh2* (24), were previously identified by functional assays to be required for expression of *sws2* and *rh2* opsin genes. These results suggest that *sws2* and *rh2* opsin genes are directly regulated by Six6b and Six7.

We next searched for other target genes of Six6b and Six7, defining targets by the presence of ChIP-seq signal near the transcription start site (*Materials and Methods*). This analysis revealed that Six6b and Six7 had a considerable number of common target genes (Fig. 4*C*), which included those encoding components of the cone-specific phototransduction cascade downstream of opsins, such as *gnat2* and *pde6c* (*SI Appendix*, Fig. S5 *A–C*). These observations suggest that Six6b and Six7 similarly contribute to transcriptional regulation essential for cone function. The great number of common binding sites between Six6b and Six7 (Fig. 4*D*) raised the possibility that they recognize similar DNA sequences. To characterize the DNA-binding specificities of Six6b and Six7, the binding sites of Six6b and Six7 (Fig. 4*D*) were subjected to motif analysis by HOMER (25). We found that the overrepresented binding motifs of Six6b and Six7 were highly similar to each other (Fig. 4*E*), while the Six6b-binding motif [TNA(T/G)C(C/T)] appeared less stringent than that identified in a prior study analyzing the in vitro-binding preference of mouse Six6 (TAATCC) (26). To characterize Six6b- and Six7-binding motifs in detail, we adopted an unbiased bioinformatics method called motif centrality analysis of ChIP-seq (MOCCS) that we developed previously (27, 28). This method takes advantage of the fact that significant DNA-binding motifs of transcription factors should frequently appear at the center of their binding sites identified by ChIP-seq. MOCCS explicitly evaluates which sequence is used (and to what extent) in a genome-wide and unbiased manner (27, 28), contrasting with previous methods for motif analysis. Considering that HOMER analysis predicted 6-mer motifs for both Six6b and Six7 binding (Fig. 4*E*), we drew a histogram of the appearance of each 6-mer motif around the binding sites using the full complement of Six6b- or Six7-binding sites (details are provided in refs. 27, 28). For binding motifs showing a sharp peak in the histogram, we drew a cumulative relative frequency curve and calculated the area under the cumulative relative frequency curve (termed AUC) to quantify the sharpness of the peak. It should be noted that when a peak becomes sharper, the AUC becomes larger (Six6b-binding motifs with the top 10 AUC scores are shown in Fig. 4*F*). When the AUC scores of each 6-mer motif were compared between Six6b and Six7, we found a positive correlation between the binding motifs showing higher AUC scores (Fig. 4*G*, motifs 1–10). The motif with the highest AUC score (TAATCC) for both Six6b and Six7 was identical to the consensus binding motif of Crx (29). Our MOCCS analysis of previously published ChIP-seq data for mouse Crx (29) revealed that some of the top 10 motifs of Six6b binding were highly correlated with those of Crx binding (Fig. 4*H*), indicating that Six6b, Six7, and Crx share common binding motifs (motifs 1, 2, 3, 7, and 9). These motifs showed far lower AUC scores for homeobox transcription factor Cdx4 (30) (Fig. 4*I*), which is distantly related to Six and Crx, supporting the reliability of Six6b-binding specificities determined by MOCCS. Collectively, similarities in the binding motifs and the target genes between Six6b and Six7 suggest their common role(s) for transcriptional regulation of cone photoreceptor genes. In addition, the similarity

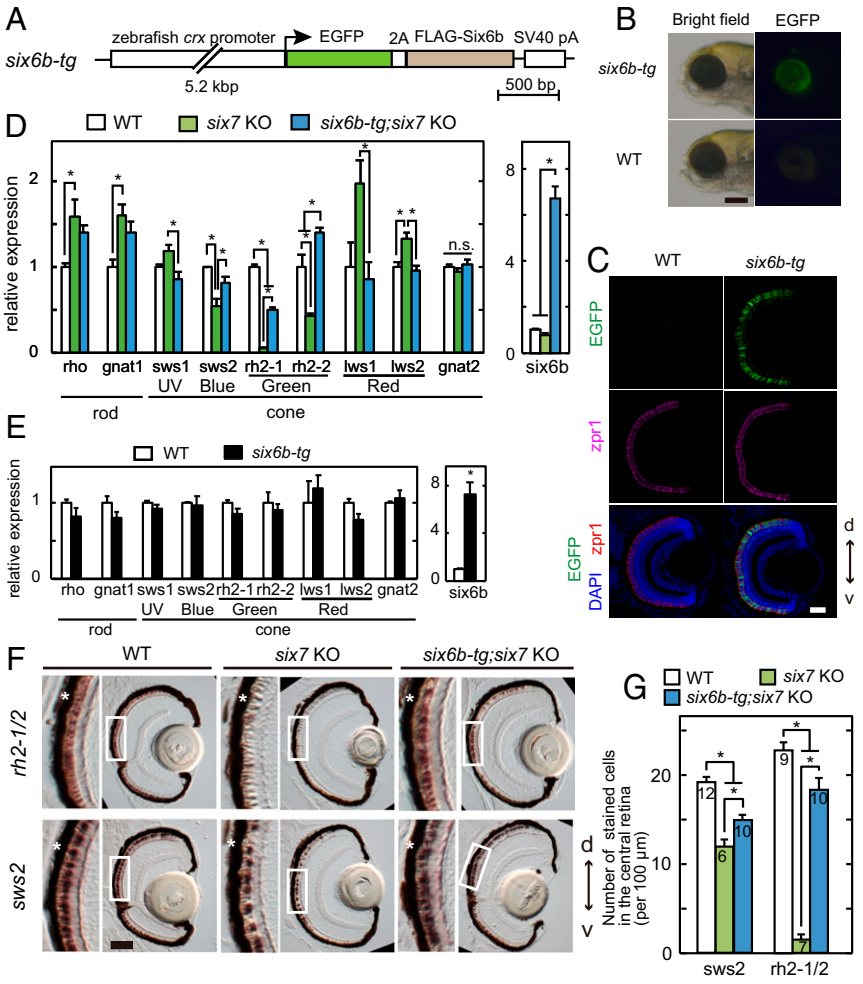

Fig. 3. Compensatory regulation of *sws2* and *rh2* opsin genes by *six6b* and *six7*. (*A*) Schematic drawing of the transgene construct. (*B*) EGFP expression in the anterior region of *six6b-tg* (ja70Tg) at 5 dpf. (Scale bar: 200 μm.) (*C*) EGFP signals detected in retinal photoreceptor layers of 4-dpf *six6b-tg* larvae (*green*). Weak EGFP signals were also detected in the inner nuclear layer (also *SI Appendix*, Fig. S2*A*), consistent with previous work (12). RH2 and LWS cones were labeled with zpr1 antibody (magenta). Cell nuclei were counterstained with DAPI (blue). (Scale bar: 40 μm.) (*D* and *E*) Relative mRNA levels of opsin genes and *six6b* in the 5-dpf larval eyes [mean ± SEM, $n = 4$ independent samples analyzed for each genotype; $^*P < 0.05$, Tukey's multiple comparison test (*D*), Student's *t* test (*E*)]. n.s., not significant. (*F*) Expression pattern of cone opsin genes examined by in situ hybridization using the 5-dpf larval eyes. Magnified view of the photoreceptor layer (box surrounded with white lines) is indicated on the left side of each panel. The retinal pigmented epithelium is indicated by asterisks. *d*, dorsal side; *v*, ventral side. (Scale bar: 50 μm.) (*G*) Related to *F*. Quantification of *sws2*- or *rh2-1/2*–positive photoreceptors in the central retina (mean ± SEM; $^*P < 0.05$, Tukey's multiple comparison test). The numbers of fish used for quantification are indicated in the bar graph.

of their binding preferences to that of Crx suggests that *sine oculis* transcription factors may have been coopted for cone subtype gene regulation in the course of evolution on account of their ability to act upon preexisting Crx-binding sites.

Coordinated Regulation of *sws2* Opsin Gene Expression by Six6 and Six7. We next asked whether *six6b* and its paralog, *six6a*, play a role in the regulation of *sws2* and *rh2* opsin expression. We generated *six6a* and *six6b* KOs using TAL effector nucleases (Fig. 5 *A* and *B*), and quantified the ocular mRNA levels of genes for phototransduction components, including opsins. Compared with control fish, no significant alteration of the mRNA level of any visual opsin gene was detected in the following mutants: *six6a* KO, *six6b* KO, or *six6a*/*six6b* double KO (DKO; Fig. 5 *C* and *D*). The mutant fish were then crossed with *six7* KO, in which *sws2* opsin gene expression was significantly reduced, as we previously reported (17) (*SI Appendix*, Fig. S6). The *six6a*/*six6b*/*six7* TKO zebrafish larvae exhibited the most severe reduction in mRNA level of both green (*rh2-1* and *rh2-2*) and blue (*sws2*) cone opsins (Fig. 5*D*). The mRNA signals for *sws2* and *rh2* cone opsins were undetectable by in situ hybridization in the larval TKO retina (Fig. 5*E*), where the laminar structure appeared normal (*SI Appendix*, Fig. S7). Severe reduction in *sws2* opsin mRNA was also observed in the larvae of two independent lines of *six6b*/*six7* DKO fish (*SI Appendix*, Fig. S6), as well as in adult TKO fish (*SI Appendix*, Fig. S8). Collectively, we conclude that both *six6b* and *six7* are essential for the expression of middle wavelength-sensitive blue (*sws2*) and green (*rh2*) cone opsins.

Disordered Cone Mosaic in *six6a*/*six6b*/*six7* TKO Fish. Next, we examined the cone mosaic by immunofluorescent labeling of RH2-LWS double cones with zpr1 antibody (31) in the flat-mounted retina of adult TKO fish. In contrast to the ordered array of double cones in WT retina, we found that the double-cone array was markedly disrupted in TKO fish (Fig. 5*F*). To evaluate cone survival in the disordered mosaic, we performed transferase-mediated dUTP nick-end labeling (TUNEL) on TKO adult retinas and controls (Fig. 5*G*). A significant increase in TUNEL-positive signals was observed in TKO retina, especially in the far periphery, a region that includes the ciliary marginal zone where proliferating cells reside (20). It is likely that Six6 and Six7 together play an essential role in the development of SWS2 and RH2 cones in addition to controlling expression of SWS2 and RH2 opsins.

Impaired Foraging Behavior in *six6a*/*six6b*/*six7* TKO Larvae. While rearing larvae with various combinations of *six6a*, *six6b*, and *six7* KO alleles, we noticed that only a few of the *six7* KO larvae and none of the TKO larvae survived into adulthood (*SI Appendix*, Fig. S9*A*). In contrast, the expected Mendelian proportion of mutants was observed at the 5-dpf larval stage (*SI Appendix*, Fig. S9*B*), indicating that TKO larvae completed normal embryonic development but did not survive afterward under conditions of mass rearing. We found that higher population density in the fish tank resulted in smaller numbers of adult *six7* KO fish (and the double and triple mutants that included *six7* deficiency) and a correspondingly smaller body size in the survivors, suggesting that the mutants failed to compete successfully for food. We hypothesized that *six7* KO and its derived mutants could be raised into adulthood by rearing them separately from the others

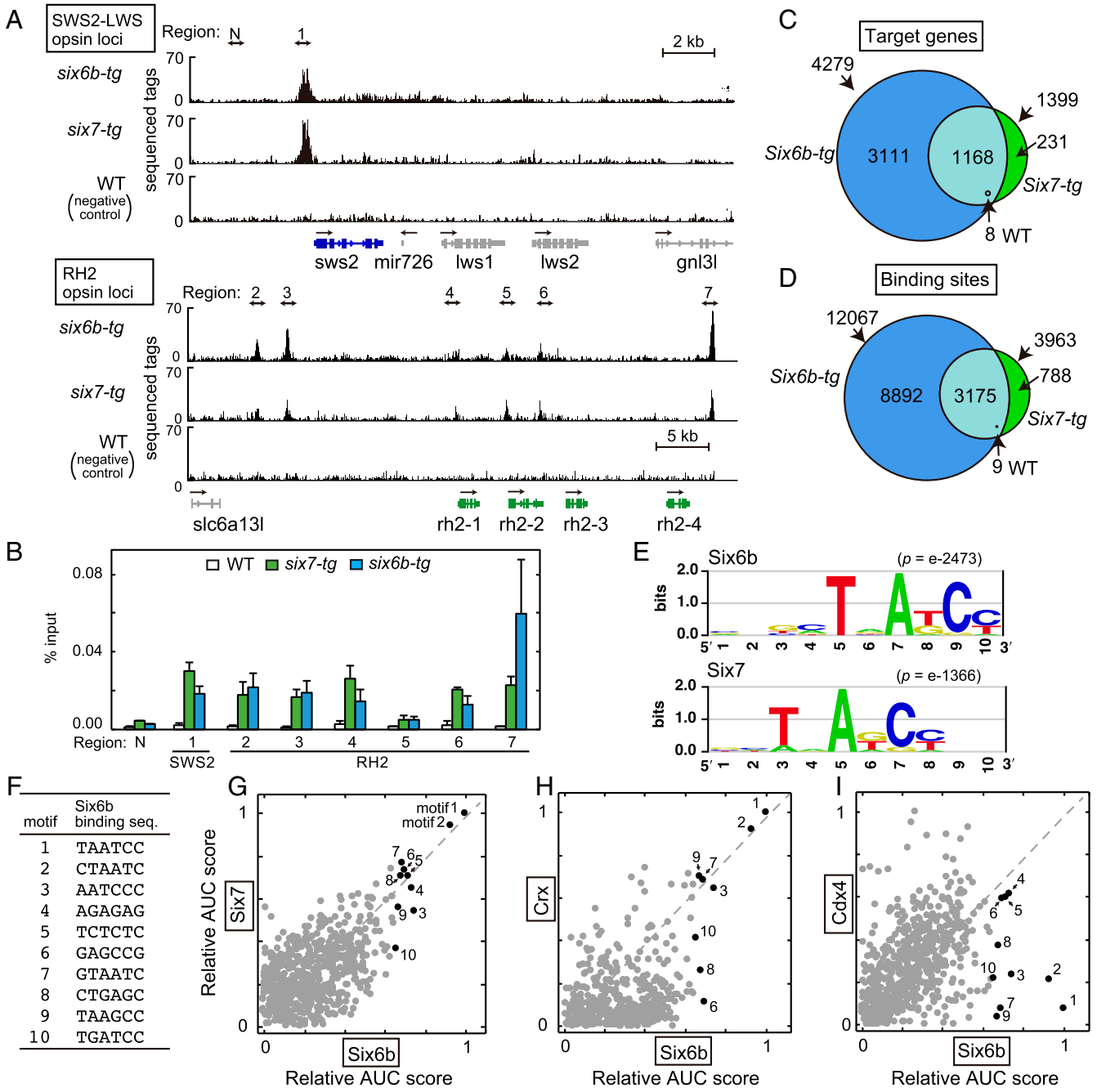

Fig. 4. DNA-binding specificities of Six6b and Six7. (*A*) Visualization of Six6b and Six7 ChIP-seq peaks obtained from the adult retina of *six6b-tg* (ja70Tg), *six7-tg* (ja69Tg), and WT with the anti-FLAG antibody. (*B*) ChIP-qPCR signals obtained from the adult retina of *six6b-tg*, *six7-tg*, and WT (mean ± SD, $n = 2$). The amplified genome regions (regions 1–7 and N) are indicated in *A*. Note that the ChIP-qPCR analysis was conducted using the samples prepared independently from the ChIP-seq analysis. (*C*) Overlap of Six6b and Six7 target genes. (*D*) Overlap of Six6b- and Six7-binding sites. (*E*) Overrepresented binding motifs determined by HOMER. (*F*) Top 10 motifs of Six6b binding. (*G–I*) Scatter plots comparing relative AUC scores of 6-mer motifs among the ChIP-seq datasets. The AUC scores of each motif were normalized to the highest AUC score for each dataset. The normalized scores were plotted in the graph if they were greater than 0. The top 10 motifs of Six6b binding are indicated in the graph.

after they start to feed (at around 6 dpf). To identify the disadvantaged population (*six7* KO, *six6a/six7* DKO, *six6b/six7* DKO, and TKO), a SWS2 cone-specific EGFP transgene, *Tg (-3.5opn1sw2:EGFP)*^{kj11Tg}, was crossed onto the mutant backgrounds (23). This transgene permitted us to readily identify the disadvantaged larvae as those showing lower levels of green fluorescence in the eye. By isolating these larvae, we obtained markedly increased numbers of the disadvantaged adult mutants, including the TKO (*SI Appendix*, Fig. S9*C*). This finding indicates that isolated rearing of the mutants relieved competition for food, permitting greater survival to adulthood.

Next, we directly evaluated the foraging behavior of mutant larvae by examining visual prey capture of TKO larvae at 6 dpf (Fig. 6*A* and *SI Appendix*, Fig. S10). We found that paramecium (prey) consumption was significantly reduced in TKO larvae compared with WT (Fig. 6 *B* and *C* and Movie S1). Consistently, TKO larvae exhibited a significant reduction in frequency of a specialized oculomotor behavior (Fig. 6 *D* and *E*), termed "eye convergence,"

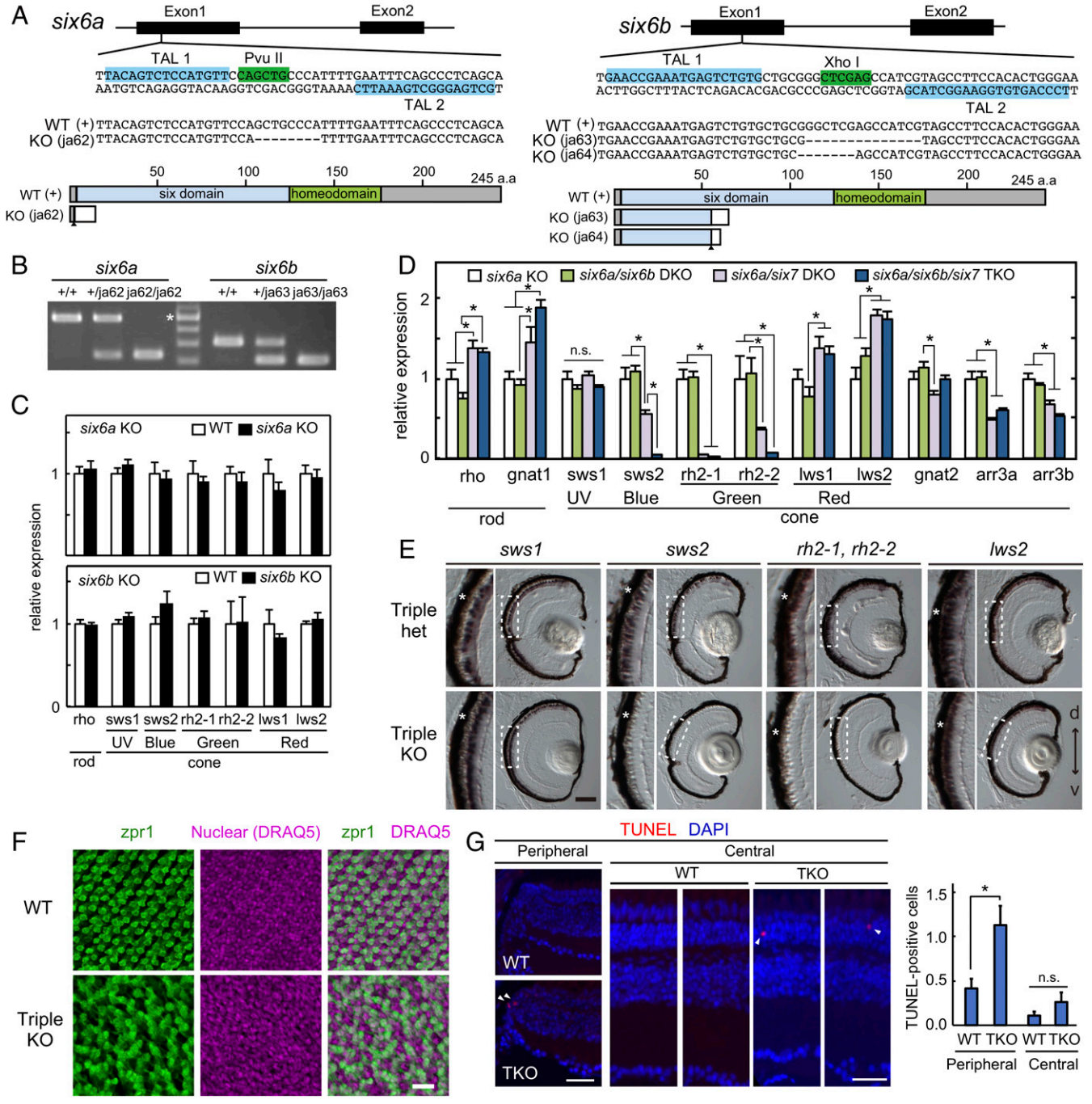

Fig. 5. Compromised development of cone photoreceptors in *six6a/six6b/six7* TKO zebrafish. (*A*) Exon/intron organization and partial nucleotide sequences of zebrafish *six6a* and *six6b*. The binding sites of the left and right TAL effector nucleases are highlighted in blue. The recognition sites of the restriction endonucleases PvuII and XhoI are highlighted in green. The nucleotide sequences of the KO fish alleles (ja62 for *six6a*, ja63 and ja64 for *six6b*) are compared with the WT sequence. Deletions are indicated by dashes. Six6a and Six6b and their mutant proteins are represented as schematic drawings. The frameshift position is indicated by an arrowhead. (*B*) Genotyping of the *six6a* and *six6b* mutants by PCR. The asterisk indicates 500 bp. Expression profiles of rod and cone opsin genes in the larval eyes at 4 dpf (*C*; mean ± SEM, $n = 4$ for each genotype; $^*P < 0.05$, Student's *t* test) and at 5 dpf (*D*; mean ± SEM, $n = 5$ for each genotype; $^*P < 0.05$, Tukey's multiple comparison test) are shown. n.s., not significant. The *n* value refers to the number of independent samples analyzed. (*E*) Expression pattern of cone opsin genes examined by in situ hybridization using 5-dpf larval eyes. A magnified view of the photoreceptor layer (dotted box) is indicated on the left side of each panel. The retinal pigmented epithelium is indicated by asterisks. *d*, dorsal side; *v*, ventral side. (Scale bar: 50 μm.) (*F*) Fluorescent images of the flat-mounted retinas prepared from the adult WT and TKO. The retinas were immunostained with zpr1 antibody, which recognizes RH2 and LWS cones (*green*) and with DRAQ5 to highlight cell nuclei (magenta). (Scale bar: 20 μm.) (*G*, *Left*) Fluorescent images in retinal cryosections from the adult fish labeled for TUNEL (red). The cell nuclei were counterstained with DAPI (blue). TUNEL-positive cells are indicated by arrowheads. (Scale bars: 30 μm.) (*G*, *Right*) Quantification of TUNEL-positive cells in the central or peripheral retina. The numbers of TUNEL-positive cells were counted for each cryosection and averaged (mean ± SEM, $n = 55$ for WT, $n = 38$ for TKO; $^*P < 0.05$, Student's *t* test vs. WT). n.s., not significant.

which is closely associated with prey capture (32). Note that the behavioral assay was conducted under white LED light covering a broad range of visible light (*SI Appendix*, Fig. S10*C*), which is expected to stimulate all four classes of cone opsins in larval zebrafish. Nevertheless, the TKO mutant failed to demonstrate effective foraging behavior (Fig. 6), probably due to a severe reduction in gene expression of middle wavelength-sensitive blue (SWS2) and green (RH2) opsins (Fig. 5). We observed no significant alteration of locomotor activity, such as swimming speed, in TKO larvae (Fig. 6*F*), suggesting that the motor system is unaffected by the mutations. Taken together, these results demonstrate that Six6b and Six7 coordinately regulate *sws2* and *rh2* expression, and therefore play a critical role in mediating visually guided behaviors required for survival under mass rearing conditions.

Discussion

In the present study, we found that *six6b*, a transcription factor that is widely conserved among vertebrates, showed a cone-enriched pattern of expression. We demonstrated that *six6b* is capable of driving *rh2* opsin gene expression even in the absence of *six7* (Fig. 3), a transcription factor present only in the ray-finned fish lineage and essential for *rh2* gene expression. ChIP-seq analysis (Fig. 4) indicated that Six6b and Six7 share binding preferences and numerous target genes in zebrafish photoreceptors. Loss-of-function experiments (Fig. 5) revealed that *six6b* and *six7* coordinately regulate *sws2* gene expression. Together, these results demonstrate complementary regulation of middle wavelength-sensitive SWS2 and RH2 opsin expression by Six6b and Six7. Importantly, the *six6* gene is widely conserved among vertebrate species having these opsin genes (18, 33) (Fig. 1), raising the possibility that Six6 is a key transcriptional regulator of SWS2 and RH2 expression in the vertebrate species that lack *six7*. Consistent with this notion, we found *Six6* expression in RNA-sequencing data from cone cells purified from cultured chicken retinas (34). Loss-of-function experiments with chicken embryos using in vivo electroporation (35) could facilitate understanding of the role(s) of avian Six6 for SWS2 and RH2 opsin gene expression.

ChIP-seq and bioinformatic analysis (Fig. 4*F*) indicate that Six6b and Six7 share binding preferences with Crx, suggesting that they regulate cone gene expression, at least in part, by binding Crx target motifs. Crx is a master transcriptional regulator for the development of both rod and cone photoreceptors (10, 11), while Six6b and Six7 regulate gene expression mainly in middle wavelength-sensitive blue (SWS2) and green (RH2) cones. The discrete roles of Crx and Six6b/Six7 suggest that, in addition to the motifs shared by Crx and Six6b/Six7, there may be other motifs specific to Six6b/Six7 that play an important role in regulating gene expression in SWS2 and RH2 cones. Although the current study revealed transcription factors required for *sws2* and *rh2* opsin expression, it remains unclear how Six6b and Six7, although expressed broadly among cone subtypes, can drive subtype-specific gene expression and how mutually exclusive expression of *sws2* and *rh2* opsins is established. Further studies are required to identify transcription factor(s) specifying SWS2 and RH2 cones and to unveil a mechanism underlying differentiation between them.

In the present study, we found that *rh2* genes have multiple binding sites for Six6b and Six7 in both proximal and distal regions, including in the so-called "locus control region" (region 3 in Fig. 4*A*), which regulates expression of the tandemly arrayed *rh2* genes in zebrafish (24). The *rh2*, *sws2*, and *lws* genes are often duplicated in teleost fishes (Fig. 1) and often reside in tandem arrays (36). Interestingly, the *six7* gene is present only in the ray-finned fish lineage (17) (Fig. 1), suggesting that *six7* contributes to transcriptional regulation of the tandem arrays of *rh2* genes. The duplicated RH2 opsins have distinct wavelength sensitivities and show expression patterns spatiotemporally distinct from each other (22, 36). Six7-mediated regulation of tandemly arrayed *rh2* genes could therefore be key for their differential gene expression.

A previous study in mice reported that *Six6* deficiency caused severe retinal abnormalities as well as abnormalities of the optic chiasma and optic nerve (37). These phenotypes of *Six6* KO mice

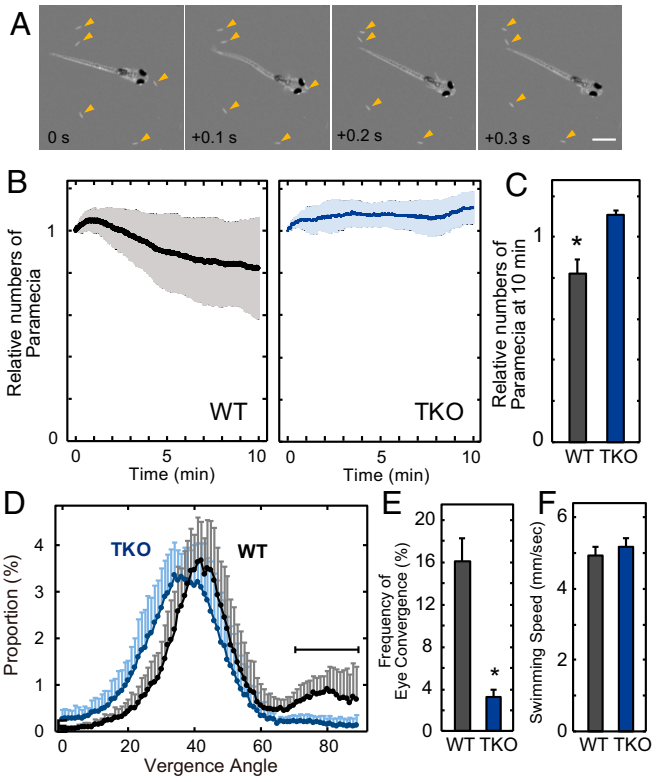

Fig. 6. Impaired prey capture in *six6a/six6b/six7* TKO zebrafish at 6 dpf. (*A*) Time-lapse images during a typical hunting episode. Paramecia are indicated by orange arrowheads. (Scale bar: 100 μm.) (*B*) Relative numbers of paramecia counted in the chamber containing WT and TKO larvae. The number of the paramecia left in the chamber was normalized to the initial count. The data are represented by mean ± SD (n = 12 for each genotype). (*C*) Relative numbers of paramecium at 10 min (mean ± SEM, n = 12; $^*P < 0.05$, Student's t test). (*D*) Distribution of eye vergence angle. The data are represented by mean ± SD (n = 12). (*E*) Frequency of eye convergence during 10 min. The eye convergence was defined as the state in which the eye vergence angle was more than 70°. A vergence angle greater than 70° is indicated by the bar in *D*. (*F*) Swimming speed of WT and TKO larvae. Values in *E* and *F* are presented as mean ± SEM (n = 12; $^*P < 0.05$, Student's t test).

have made it difficult to examine whether mouse *six6* is engaged in later stages of retinal development, such as development and maintenance of cone photoreceptors. In zebrafish, no obvious defects were observed in the laminar structure of the *six6a/six6b/six7* TKO retina (Fig. 5*E* and *SI Appendix*, Figs. S7 and S8*C*), suggesting that early ocular development might be redundantly regulated by Six6 and other factor(s). Thus, the zebrafish is a suitable animal model for investigating the role of *six6* in later retinal development. Our present study identified zebrafish *six6* as a crucial regulator of *sws2* and *rh2* opsin expression. Gene ontology analysis of the target genes common to Six6b and Six7 identified not only cone signal transduction genes (Fig. 4 *A* and *B* and *SI Appendix*, Fig. S5 *A*–*C*) but also others important for neurogenesis and neuronal development (*SI Appendix*, Fig. S5*D*). We also found disordered cone mosaic in the TKO retina (Fig. 5*F*) and increased cell death in the peripheral region (Fig. 5*G*). Collectively, these results suggest that zebrafish *six6* and *six7* contribute to retinal cone development, including fate choice of cone subtypes at the precursor stage. It was reported that cone subtype identity is defined before terminal cell division of the cone precursors (12). In fact, *six6b* expression was observed not only in the photoreceptor layer but also in the peripheral region of larval retina (Fig. 2*E*), where proliferating cells reside. Further analysis of the target genes of Six6b and Six7 would be valuable for understanding mechanisms underlying coordination of cone photoreceptor development.

We observed that TKO fish show reduced adult survival after mass rearing due to severely impaired foraging behavior. A previous study reported that mutant zebrafish lacking UV (SWS1) cones (*tbx2b* mutant) also exhibited impaired foraging behavior (38). We should note that TKO fish had no obvious defects in *sws1* opsin expression (Fig. 5*D*) but were deficient for blue (*sws2*) and green (*rh2*) opsins (Fig. 5 and *SI Appendix*, Figs. S6 and S8). Our behavioral tests indicate that the two opsin subfamilies covering middle-wavelength sensitivity (SWS2 and RH2) play a key role in mediating visually guided behavior in larval zebrafish. Paradoxically, the genes encoding *sws2* and *rh2* opsins have been lost in mammalian species, most likely due to a long evolutionary history of nocturnality in mammalian ancestors (39). In almost all eutherian mammals, however, amino acid substitutions have given rise to spectral tuning of a subset of cone opsins and, consequently, have shifted their light sensitivities toward the middle-wavelength (blue and green) region (40). The λ_{max} of UV (SWS1) opsin is shifted toward the blue region (e.g., 360 to 420 nm) in almost all eutherian mammals except for rodents (41), while in rodents, the λ_{max} of the red (LWS) opsin is shifted toward the green region (e.g., 560 to 500 nm) (42). These spectral shifts (spectral convergence into the middle-wavelength region) suggest that light sensitivity in the middle-wavelength (blue and green) region is physiologically important at least for daylight vision, as the middle-wavelength region of solar light is enriched in both terrestrial and aquatic environments (43).

Materials and Methods

Zebrafish. All research described here adhered to local guidelines of the University of Tokyo, and all appropriate ethical approval and licenses were obtained from Institutional Animal Care and Use Committees of The University of Tokyo. Ekkwill strain zebrafish were raised in a 14-h light/10-h dark cycle. The larval zebrafish were fed once per day with artificial fish food, Kyowa N250 (Kyowa Hakko Kogyo) from 5 to 10 dpf, and larvae older than 10 dpf were fed twice per day with live baby brine shrimps. Embryos were raised at 28.5 °C in egg water (artificial seawater diluted 1.5:1,000 in water). For effective detection of EGFP expression in the transgenic zebrafish (Fig. 3*B* and *SI Appendix*, Fig. S3*A*), the larvae were treated with fish water containing 0.003% 1-phenol-2-thiourea (PTU) from 24 h after fertilization to block synthesis of melanin pigment.

The ages of adult zebrafish used are listed in *SI Appendix*, Table S2, and the mating pairs used are shown in *SI Appendix*, Table S3. In each experiment, we used zebrafish of similar body size. We also used similar male/female ratios when comparing groups with different genotypes.

Isolation of EGFP-Positive Larvae. For isolation of transgenic larvae lacking SWS2 cones, we raised PTU-treated larvae until 5 dpf and identified transgenic larvae by EGFP expression in the eyes or a region of the brain (23). It should be noted that the brain expression of EGFP in the transgenic larvae was observed even in the *six6a/six6b/six7* KO fish. We then separated the transgenic larvae showing reduced numbers of SWS2 cones from the others by ocular EGFP fluorescence and raised the two separated groups (weak or normal EGFP expression) to adulthood.

Mutant Zebrafish. The *six6a* and *six6b* mutant zebrafish lines were generated as described previously (17). Detailed information about the methods used to generate mutant zebrafish is provided in *SI Appendix*, *Methods*. In this paper, *six6a*$^{ja62/ja62}$, *six6b*$^{ja63/ja63}$, and *six7*$^{ja51/ja51}$ zebrafish are referred to as *six6a*, *six6b*, and *six7* KO zebrafish, respectively, except for in *SI Appendix*, Fig. S6.

Plasmid Construction. Detailed information about the methods used for plasmid construction is provided in *SI Appendix*, *Methods*. The DNA sequence data for *six6b*- and *six7*-expressing plasmids are available from the DNA Data Bank of Japan (DDBJ)/European Molecular Biology Laboratory (EMBL)/National Center for Biotechnology Information (NCBI) [accession nos. LC413281 (Six7) and LC413282 (Six6b)].

Generation of Transgenic Zebrafish. Detailed information about the methods used for generation of transgenic zebrafish is provided in *SI Appendix*, *Methods*.

Immunofluorescent Labeling of Ocular Cryosections. Immunohistochemistry on ocular sections was performed essentially as described previously (17), with some modifications. In short, the larvae were dissected into anterior and posterior segments; the posterior segments were used for the genotyping, while the anterior segments were subjected to cryosectioning. The larval anterior segments, or adult eyes, were fixed in 4% paraformaldehyde (PFA) in Ca^{2+}- and Mg^{2+}-free Dulbecco's PBS (D-PBS) overnight at 4 °C. After sucrose infiltration and optimal cutting temperature compound embedding, the treated samples were frozen and sectioned on a cryostat at a thickness of 10 μm. The sections on the glass slides were soaked with a blocking solution (3% goat normal serum, 0.1% Triton X-100 in D-PBS) and then incubated with a primary antibody diluted in the blocking solution. The sections were further incubated with a secondary antibody in the presence of 3 μg/mL DAPI for staining of the cell nuclei. The treated sections were coverslipped with VECTASHIELD Mounting Medium (Vector Laboratories) and examined with a confocal laser scanning microscope (TCS SP8; Leica). The primary antibodies used were as follows: mouse monoclonal antibody zpr1 (diluted 1:400; Zebrafish International Resource Center) (31) specific to arrestin 3a, which is a cone phototransduction protein expressed in double cones (RH2 and LWS cones), and rabbit polyclonal antibody against rod transducin α-subunit, Gnat1 (sc-389, diluted to 0.5 μg/mL; Santa Cruz Biotechnology). The secondary antibodies used were goat anti-mouse IgG antibody conjugated with Alexa-568 (A-11004, diluted to 2 μg/mL; Molecular Probes), goat anti-rabbit IgG antibody conjugated with Alexa-488 (A-11034, diluted to 2 μg/mL; Molecular Probes), and/or goat anti-mouse IgG antibody conjugated with Alexa 647 (A-21236, diluted to 2 μg/mL; Molecular Probes).

Immunofluorescent Labeling of Flat-Mounted Retina. Immunofluorescent labeling of flat-mounted retina was carried out as described (44), with some modifications. Briefly, retinas were isolated from dark-adapted adult zebrafish, and each of the retinas was processed to have four small radial cuts with equal spacing. Each retina was placed onto a piece of Parafilm sheet in an ∼50-μL drop of fixative (4% PFA in D-PBS with 5% sucrose). The retina was immediately covered with another piece of Parafilm sheet, over which a 1.5-g weight (1.5-mL tube containing water) was placed. After 45 min of incubation at room temperature, the flattened retina was placed in 1 mL of fixative for another 45 min at room temperature. After the fixation, the retina was washed with 5% sucrose in D-PBS three times for 20 min each time and then placed in 300 μL of antibody diluent (1% Triton X-100, 1% Tween 20, 1% DMSO in D-PBS) containing the zpr1 antibody (diluted 1:100) for ∼20 h at room temperature. The retina was then washed with the antibody diluent three times for 10 min each time and treated with goat anti-mouse IgG antibody conjugated to Alexa 568 (A-11004, diluted to 10 μg/mL; Molecular Probes) in the antibody diluent for ∼20 h at room temperature. This second antibody reaction was performed in the presence of 10 μM DRAQ5 (DR5050; BioStatus) for staining of the cell nucleus. The retina was then washed with the antibody diluent three times for 10 min each time, mounted onto an agarose-coated slide glass with the photoreceptor layer facing down, and coverslipped with VECTASHIELD Mounting Medium. Fluorescent images of the immunostained retina were captured with a TCS SP8 confocal laser scanning microscope.

TUNEL Staining. One head of an adult fish was subjected to cryosectioning for each genotype in a single experiment. Frozen ocular sections (10 μm thick) were prepared as described in the previous section. The cryosections were subjected to TUNEL staining by using the Click-iT TUNEL Alexa Fluor 594 Kit (Invitrogen) according to the manufacturer's protocol. The stained sections were coverslipped with VECTASHIELD Mounting Medium with DAPI (Vector Laboratories) and observed with a microscope (Axioplan2; Carl Zeiss).

In Situ Hybridization. The cRNA probes were generated as described in our previous study (17). The sequences of *sws1*, *sws2*, *rh2-1*, *rh2-2*, and *lws2* cRNA probes were described in our previous study (17). For detection of all of the *rh2* opsin genes expressed at the larval stage, the cRNA probe was designed in the coding region of *rh2-2* to recognize both *rh2-1* and *rh2-2* opsin genes (referred to here as *rh2-1/2*). Alternatively, we used a mixture of two different RNA probes, each of which specifically recognizes either the *rh2-1* or *rh2-2* opsin gene. The *six6b*_5UC cRNA probe (used in Fig. 2 *D* and *E*) was designed in the region containing the 5′ UTR and coding sequence of *six6b*, while the *six6b*_C cRNA probe (used in Fig. 2*F*) was designed in the coding sequence of *six6b*. PCR primers utilized to amplify the target gene fragments used to prepare cRNA probes are listed in *SI Appendix*, Table S4.

Whole-mount in situ hybridization was carried out essentially as described previously (17). Briefly, larval zebrafish were fixed in 4% PFA in D-PBS overnight at 4 °C and dehydrated in methanol. The samples were rehydrated and pretreated with proteinase K. The treated larvae were hybridized with the digoxigenin (DIG)-labeled RNA probes, and the hybridization signals were visualized by nitro-blue tetrazolium and 5-bromo-4-chloro-3′-indolyphosphate

(NBT/BCIP) staining. After staining, the specimens were immersed in glycerol and examined with a stereoscopic microscope (MZ-FL3; Leica).

In situ hybridization using larval and adult ocular sections was carried out essentially as described previously (17). Briefly, the 10-μm frozen ocular sections were prepared as described above. The cryosections were pretreated with proteinase K and hybridized with the DIG-labeled RNA probes, and the hybridization signals were visualized by NBT/BCIP staining. The treated slides were examined with a microscope (Axioplan2; Carl Zeiss).

Behavioral Assay for Prey Capture. Detailed protocols and a tutorial movie for the prey capture behavior assay can be found in our previous studies (45, 46). One zebrafish larva (6 dpf) was placed in a recording chamber (diameter, 20 mm; depth, 2.5 mm; CoverWell Imaging Chambers PCI-A-2.5, Grace Bio-Labs), which was attached onto a glass slide. Approximately 40 paramecia (*Paramecium caudatum*) were placed in the recording chamber, with a cover glass on top. The recording chamber was illuminated with a white LED light (LDR2-100SW2-LA; CCS, Inc.) that was placed under the recording chamber. Light intensity at the recording chamber was set at ∼10,000 lux, in which rod responses should be mostly saturated and would not contribute to visually guided behavior. In this lighting condition, paramecia looked white and larval zebrafish eyes appeared black on the gray background. The larva and paramecia were imaged using a stereoscope (SZX7; objective lens, DF PL 0.5×; Olympus) equipped with a complementary metal–oxide–semiconductor camera (xiQ; product no. MQ042RG-CM; Ximea). Image acquisition was controlled by custom-made software developed on LabVIEW with the xiLIB toolkit (a LabVIEW interface for Ximea cameras). After time-lapse recordings (for 11 min taken at 10 frames per second), the number of paramecia in the chamber was counted for each frame using the particle analysis function in ImageJ (https://imagej.nih.gov/ij/). To circumvent the unwanted technical variation among individual frames, we averaged the number of paramecia for the 600-frame time bin that corresponds to a 1-min interval and examined how many paramecia were consumed over minutes. The swimming speed and eye vergence angle of the larval zebrafish were measured in ImageJ using the Moment Calculator plug-in. Eye convergence was defined as the state in which the eye vergence angle was more than 70° (32).

Photoreceptor Isolation. The transgenic zebrafish lines used for photoreceptor isolation were *Tg*(*rho:egfp*)^{ja2} (47) and *Tg*(*gnat2:egfp*)^{ja23} (17), which express EGFP in rods and all of the subtypes of cones, respectively. Photoreceptor isolation was carried out as described previously (17). Briefly, adult retinas were dissected in ice-cold PBS from dark-adapted adult fish under dim red light. The isolated retinas were dissociated into cell suspensions with 0.25% trypsin and 10 units/mL DNaseI in Ca^{2+}-free Ringer's solution. This reaction was terminated by adding soybean trypsin inhibitor (final 0.5%) and FBS [final 10% (vol/vol)]. The samples were filtrated through a 35-μm nylon mesh and subjected to cell sorting with a fluorescence-activated cell sorter (FACSAria; BD Biosciences). EGFP-positive photoreceptors were separated by the following three parameters: forward scatter, side scatter, and green fluorescence. The sorted cells were directly collected into 800 μL of TRIzol reagent (Thermo Fisher Scientific) in 1.5-mL microtubes. The numbers of collected photoreceptors were ∼600,000 cells (rod sample 1), ∼750,000 cells (rod sample 2), ∼180,000 cells (cone sample 1) and ∼200,000 cells (cone sample 2). The total RNA was purified using a RNeasy MinElute Cleanup Kit (Qiagen). An equal amount of RNA from each sample was reverse-transcribed with SuperScript II (Thermo Fisher Scientific) using anchored $(dT)_{16}$ primers.

RNA Extraction and cDNA Preparation from Enucleated Eyes. All of the zebrafish were sampled during the light phase of the light/dark cycle. The adult fish eyes were soaked in RNA*later* (Sigma) and stored at 4 °C. The larvae were dissected into anterior and posterior segments; the posterior segments were used for genotyping, while the anterior segments were soaked in RNA*later* and stored at 4 °C. After genotyping, the larval eyes were isolated with a needle. Two larval eyes (or one adult eye) were considered a biological replicate for each genotype, except in Fig. 2*C*. Total RNA was extracted and purified with a RNeasy Micro Kit (Qiagen) or RNeasy Mini Kit (Qiagen). An equal amount of RNA from each sample was reverse-transcribed into cDNA with the oligo $(dT)_{15}$ primer with GoScript Reverse Transcriptase (Promega).

RT-qPCR Analysis. Reverse-transcribed cDNA, as described above, was subjected to qPCR using GoTaq qPCR Master Mix (Promega) and the StepOnePlus Real-Time PCR System (Applied Biosystems) according to the manufacturer's protocol. Relative expression levels were calculated with a relative standard curve created with serially diluted cDNA samples reverse-transcribed from zebrafish eye total RNA. The expression levels were normalized to beta-actin 2 (*actb2*) expression levels in all of the figures. We used PCR primers designed to amplify both the *rh2-1* and *rh2-2* opsin genes (*rh2-1/2*) or both the *lws1* and *lws2* opsin genes (referred to here as *lws1/2*) for detection of total expression levels of *rh2* or *lws* opsin genes at the larval stage. The primers used for qPCR are listed in *SI Appendix*, Table S4.

Immunoblot Analysis. To isolate the nuclear fraction, adult fish eyes were dissected and homogenized in ice-cold buffer A [10 mM Hepes-NaOH, 10 mM KCl, 0.1 mM EDTA, 1 mM DTT, 1 mM PMSF, 4 μg/mL aprotinin, 4 μg/mL leupeptin (pH 7.8)]. The homogenate was centrifuged (5 min at 700 × *g*), and the supernatant was discarded. The precipitate was washed with buffer A and centrifuged again, and the precipitate (nuclear fraction) was lysed in SDS/PAGE sampling buffer [10 mM Tris·HCl, 6% glycerol, 2% SDS, 50 mM DTT, 2 mM EDTA, 0.02% Coomassie Brilliant Blue R-250 (pH 6.8)]. Proteins in the nuclear fraction were separated on a gel by SDS/PAGE and transferred to a polyvinylidene difluoride membrane (Immobilon-P transfer membrane; Millipore). The blotted membrane was preincubated with 1% (wt/vol) skim milk (BD Diagnostic Systems) in Tris-buffered saline [50 mM Tris·HCl, 200 mM NaCl, 1 mM $MgCl_2$ (pH 7.4)] for 1 h at 37 °C for blocking. The membrane was then incubated with one of the primary antibodies in the blocking solution overnight at 4 °C. The bound primary antibodies were detected by horseradish peroxidase-conjugated secondary antibodies in combination with an enhanced chemiluminescence detection system using Western Lightning Chemiluminescence Reagent (PerkinElmer Life Sciences) or ImmunoStar (Wako Pure Chemical Industries). Chemiluminescent images were acquired with ImageQuant LAS 4000 Mini (GE Healthcare). The primary antibodies used were as follows: anti-FLAG antibody (F3165, diluted to 0.8 μg/mL; Sigma) and anti-H3K4me3 antibody (07-473, diluted to 1:5,000; Upstate). The secondary antibodies used were as follows: horseradish peroxidase-conjugated anti-mouse IgG (074-1816, diluted to 0.2 μg/mL; Kirkegaard & Perry Laboratories) and horseradish peroxidase-conjugated anti-rabbit IgG (074-1516, diluted to 0.2 μg/mL; Kirkegaard & Perry Laboratories).

ChIP. Twelve adult retinas of dark-adapted adult fish were dissected in ice-cold PBS under dim red light and soaked in 1% formaldehyde in D-PBS for 10 min at room temperature. The cross-linking reaction was terminated by addition of 125 mM glycine (final concentration). The treated retinas were homogenized in ice-cold buffer A. The homogenate was centrifuged (5 min at 700 × *g*), and the precipitate was resuspended and lysed in 1 mL of ice-cold cell lysis buffer [5 mM piperazine-N,N′-bis(2-ethanesulfonic acid), 85 mM KCl, 0.5% Nonidet P-40, 1 mM DTT, 1 mM PMSF, 4 μg/mL aprotinin, 4 μg/mL leupeptin (pH 8.0)] by incubation on ice for 10 min, gently mixing for a few seconds every 3 min. The lysed samples were centrifuged (5 min at 2,500 × *g*), and the nuclear pellet was resuspended in IPB2 buffer [20 mM Hepes-NaOH, 137 mM NaCl, 1 mM EDTA, 5% glycerol, 1% Triton X-100, 1 mM DTT, 1 mM PMSF, 4 μg/mL aprotinin, 4 μg/mL leupeptin (pH 7.8)] supplemented with 1% SDS. The sample was then sonicated seven times for 20 s each time, with intervals of 40 s (Branson Sonifier 450; set at 50% for duty cycle, 2 for output). The sample was centrifuged at 16,200 × *g* for 10 min at 4 °C, and the supernatant was then diluted in IPB2 buffer (to give a final concentration of 0.135% SDS). The diluted samples were incubated with 4 μg of anti-FLAG antibody (F3165; Sigma) overnight at 4 °C with gentle rotation. The treated samples were then incubated with 100 μL of protein G magnetic Dynabeads (Invitrogen) for 60 min at 4 °C. The beads were sequentially washed with the following buffers: once in IPB2 buffer, once in IPB2 buffer containing 500 mM NaCl, once in LiCl buffer [0.25 M LiCl, 1% Nonidet P-40, 1% deoxycholate, 1 mM EDTA, 10 mM Tris·HCl (pH 8.0)], and twice in TE buffer [10 mM Tris·HCl, 1 mM EDTA (pH 8.0)]. Finally, the washed beads were eluted twice with 200 μL of elution buffer (1% SDS, 0.1 M $NaHCO_3$) by shaking for 15 min at room temperature. The combined eluate (400 μL) was mixed with 16 μL of 5 M NaCl and incubated overnight at 65 °C. The sample was then mixed with 8 μL of 0.5 M EDTA, 16 μL of 1 M Tris·HCl (pH 6.5), and 1.6 μL of 10 mg/mL proteinase K, and the mixture was incubated for 2 h at 45 °C. The DNA was purified by extraction with phenol/chloroform/isoamyl alcohol (25:24:1) and ethanol precipitation.

The ChIP DNA samples were subjected to qPCR using GoTaq qPCR Master Mix and the StepOnePlus Real-Time PCR System according to the manufacturer's protocol. The primers used for qPCR are listed in *SI Appendix*, Table S4. Alternatively, the ChIP DNA samples were sequenced with an Illumina HiSeq 3000 sequencer (36 bp, single end), according to the manufacturer's protocol. The Illumina sequencing data for the ChIP-Seq are available in the DDBJ/EMBL/NCBI databases under accession no. PRJDB7218.

ChIP-Seq Data Analysis. CRX ChIP-seq data (accession no. GSE20012) (29) and Cdx4 ChIP-seq data (accession no. GSE48254) (30) were obtained from the Gene Expression Omnibus database (www.ncbi.nlm.nih.gov/geo). Zebrafish and mouse genome sequences were obtained from the UCSC Genome

Browser (GRCz10 and GRCm38; genome.ucsc.edu/). Annotated gene models were taken from the UCSC Genome Browser and Ensembl (release 91; www.ensembl.org/). The sequenced tags were mapped to the zebrafish and mouse genome using Bowtie (v1.2.1, options "-a –best –strata -m 1 -p 4") (48) with default parameters. The mapped tags were visualized using the Integrative Genomics Viewer. Peak calling was performed for each sample using the MACS2 program (v2.1.1) (49) with default settings. An overlap of binding sites between Six6b and Six7 was defined if their peak summits were located within 501 bp of each other. Six6b and Six7 target genes were assigned if any peak summits of Six6b and Six7 were located within 5 kbp upstream of the transcription start site or in the gene body. To evaluate which biological processes might be enriched in the Six6b and Six7 common target genes (Dataset S1), we used the DAVID Functional Annotation web tool (https://david.ncifcrf.gov), limiting our analysis to DAVID's GO biological process_5 category.

De novo motif discovery was performed with HOMER version 4.9 (25), with default options. The DNA sequences in the window of 200 bp around each peak summit were used as input sequences. We searched for motifs that are overrepresented in the sets of the input sequence relative to those of a background sequence, which was in the window of 200 bp at each edge of the input sequence. The resulting sequence logo was constructed using enoLOGOS (50).

MOCCS (v1.7) (27, 28) was used for enumeration of all of the 6-mer motifs in a set of binding sites. Genomic regions used for the motif calculation were 250 bp around each peak summit. We generated a cumulative relative frequency curve against distance from the peak summit and calculated the AUC for all of the 6-mer motifs, unless 6-mer motifs whose total frequencies within the 500-bp range were smaller than the expected frequency in random sequences.

Statistical Analysis. Sample sizes were determined based on prior literature and best practices in the field, and no statistical methods were used to predetermine sample size. A two-tailed unpaired *t* test was used to determine the statistical significance between two datasets (Excel). A χ^2 test was used to evaluate the statistical significance between the expected and observed distributions of the mutant genotypes (Excel). The Tukey–Kramer honestly significant difference test was used to determine the statistical significance among multiple datasets (JMP 10.0; SAS).

ACKNOWLEDGMENTS. We thank members of the Y.F. laboratory for valuable discussion, especially Dr. Hikari Yoshitane for helpful advice. We are grateful to Dr. Joseph C. Corbo (Washington University School of Medicine) for his critical comments on the manuscript and to Leo Volkov (Washington University School of Medicine) for his advice on immunofluorescent labeling of flat-mounted retinas. We thank the National BioResource Project Zebrafish for providing the transgenic line and Dr. Shoji Kawamura (The University of Tokyo) for the zebrafish *sws2* opsin transgenic line, *Tg(-3.5opn1sw2:EGFP)*^{kj117g}. We also thank members of the fluorescence-activated cell sorting core laboratory (The University of Tokyo) for help with cell sorting. This work was supported, in part, by Japan Society for the Promotion of Science (JSPS) Grants-in-Aid for Scientific Research (KAKENHI) Grants JP16J01681 (to Y.O.), JP16K20983 (to T.S.), JP15K07144 (to D.K.), JP18H04988 (to K.K.), JP24227001 (to Y.F.), and JP17H06096 (to Y.F.). Y.O. was a research fellow of the JSPS.

1. Lamb TD (2013) Evolution of phototransduction, vertebrate photoreceptors and retina. *Prog Retin Eye Res* 36:52–119.
2. Kawamura S, Tachibanaki S (2008) Rod and cone photoreceptors: Molecular basis of the difference in their physiology. *Comp Biochem Physiol A Mol Integr Physiol* 150:369–377.
3. Okano T, Kojima D, Fukada Y, Shichida Y, Yoshizawa T (1992) Primary structures of chicken cone visual pigments: Vertebrate rhodopsins have evolved out of cone visual pigments. *Proc Natl Acad Sci USA* 89:5932–5936.
4. Yokoyama S (2008) Evolution of dim-light and color vision pigments. *Annu Rev Genomics Hum Genet* 9:259–282.
5. Collin SP, et al. (2003) Ancient colour vision: Multiple opsin genes in the ancestral vertebrates. *Curr Biol* 13:R864–R865.
6. Davies WIL, Collin SP, Hunt DM (2012) Molecular ecology and adaptation of visual photopigments in craniates. *Mol Ecol* 21:3121–3158.
7. Bowmaker JK (2008) Evolution of vertebrate visual pigments. *Vision Res* 48:2022–2041.
8. Swaroop A, Kim D, Forrest D (2010) Transcriptional regulation of photoreceptor development and homeostasis in the mammalian retina. *Nat Rev Neurosci* 11:563–576.
9. Viets K, Eldred K, Johnston RJ, Jr (2016) Mechanisms of photoreceptor patterning in vertebrates and invertebrates. *Trends Genet* 32:638–659.
10. Furukawa T, Morrow EM, Cepko CL (1997) Crx, a novel otx-like homeobox gene, shows photoreceptor-specific expression and regulates photoreceptor differentiation. *Cell* 91:531–541.
11. Freund CL, et al. (1997) Cone-rod dystrophy due to mutations in a novel photoreceptor-specific homeobox gene (CRX) essential for maintenance of the photoreceptor. *Cell* 91:543–553.
12. Suzuki SC, et al. (2013) Cone photoreceptor types in zebrafish are generated by symmetric terminal divisions of dedicated precursors. *Proc Natl Acad Sci USA* 110:15109–15114.
13. Ng L, et al. (2001) A thyroid hormone receptor that is required for the development of green cone photoreceptors. *Nat Genet* 27:94–98.
14. Fadool JM, Dowling JE (2008) Zebrafish: A model system for the study of eye genetics. *Prog Retin Eye Res* 27:89–110.
15. Stenkamp DL (2007) Neurogenesis in the fish retina. *Int Rev Cytol* 259:173–224.
16. Alvarez-Delfin K, et al. (2009) Tbx2b is required for ultraviolet photoreceptor cell specification during zebrafish retinal development. *Proc Natl Acad Sci USA* 106:2023–2028.
17. Ogawa Y, Shiraki T, Kojima D, Fukada Y (2015) Homeobox transcription factor Six7 governs expression of green opsin genes in zebrafish. *Proc Biol Sci* 282:20150659.
18. Kumar JP (2009) The sine oculis homeobox (SIX) family of transcription factors as regulators of development and disease. *Cell Mol Life Sci* 66:565–583.
19. Vandepoele K, De Vos W, Taylor JS, Meyer A, Van de Peer Y (2004) Major events in the genome evolution of vertebrates: Paranome age and size differ considerably between ray-finned fishes and land vertebrates. *Proc Natl Acad Sci USA* 101:1638–1643.
20. Moshiri A, Close J, Reh TA (2004) Retinal stem cells and regeneration. *Int J Dev Biol* 48:1003–1014.
21. Zhang L, et al. (2017) Expression profiling of the retina of pde6c, a zebrafish model of retinal degeneration. *Sci Data* 4:170182.
22. Takechi M, Kawamura S (2005) Temporal and spatial changes in the expression pattern of multiple red and green subtype opsin genes during zebrafish development. *J Exp Biol* 208:1337–1345.
23. Takechi M, Seno S, Kawamura S (2008) Identification of cis-acting elements repressing blue opsin expression in zebrafish UV cones and pineal cells. *J Biol Chem* 283:31625–31632.
24. Tsujimura T, Chinen A, Kawamura S (2007) Identification of a locus control region for quadruplicated green-sensitive opsin genes in zebrafish. *Proc Natl Acad Sci USA* 104:12813–12818.
25. Heinz S, et al. (2010) Simple combinations of lineage-determining transcription factors prime cis-regulatory elements required for macrophage and B cell identities. *Mol Cell* 38:576–589.
26. Hu S, Mamedova A, Hegde RS (2008) DNA-binding and regulation mechanisms of the SIX family of retinal determination proteins. *Biochemistry* 47:3586–3594.
27. Ozaki H, Iwasaki W (2016) MOCCS: Clarifying DNA-binding motif ambiguity using ChIP-seq data. *Comput Biol Chem* 63:62–72.
28. Yoshitane H, et al. (2014) CLOCK-controlled polyphonic regulation of circadian rhythms through canonical and noncanonical E-boxes. *Mol Cell Biol* 34:1776–1787.
29. Corbo JC, et al. (2010) CRX ChIP-seq reveals the cis-regulatory architecture of mouse photoreceptors. *Genome Res* 20:1512–1525.
30. Paik EJ, et al. (2013) A Cdx4-Sall4 regulatory module controls the transition from mesoderm formation to embryonic hematopoiesis. *Stem Cell Reports* 1:425–436.
31. Larison KD, Bremiller R (1990) Early onset of phenotype and cell patterning in the embryonic zebrafish retina. *Development* 109:567–576.
32. Bianco IH, Kampff AR, Engert F (2011) Prey capture behavior evoked by simple visual stimuli in larval zebrafish. *Front Syst Neurosci* 5:101.
33. Lagman D, et al. (2013) The vertebrate ancestral repertoire of visual opsins, transducin alpha subunits and oxytocin/vasopressin receptors was established by duplication of their shared genomic region in the two rounds of early vertebrate genome duplications. *BMC Evol Biol* 13:238.
34. Enright JM, Lawrence KA, Hadzic T, Corbo JC (2015) Transcriptome profiling of developing photoreceptor subtypes reveals candidate genes involved in avian photoreceptor diversification. *J Comp Neurol* 523:649–668.
35. da Silva S, Cepko CL (2017) Fgf8 expression and degradation of retinoic acid are required for patterning a high-acuity area in the retina. *Dev Cell* 42:68–81.e6.
36. Hofmann CM, Carleton KL (2009) Gene duplication and differential gene expression play an important role in the diversification of visual pigments in fish. *Integr Comp Biol* 49:630–643.
37. Li X, Perissi V, Liu F, Rose DW, Rosenfeld MG (2002) Tissue-specific regulation of retinal and pituitary precursor cell proliferation. *Science* 297:1180–1183.
38. Novales Flamarique I (2016) Diminished foraging performance of a mutant zebrafish with reduced population of ultraviolet cones. *Proc Biol Sci* 283:20160058.
39. Heesy CP, Hall MI (2010) The nocturnal bottleneck and the evolution of mammalian vision. *Brain Behav Evol* 75:195–203.
40. Jacobs GH (2009) Evolution of colour vision in mammals. *Philos Trans R Soc Lond B Biol Sci* 364:2957–2967.
41. Yokoyama S, Shi Y (2000) Genetics and evolution of ultraviolet vision in vertebrates. *FEBS Lett* 486:167–172.
42. Yokoyama S, Radlwimmer FB (1999) The molecular genetics of red and green color vision in mammals. *Genetics* 153:919–932.
43. Cronin TW, Bok MJ (2016) Photoreception and vision in the ultraviolet. *J Exp Biol* 219:2790–2801.
44. Salbreux G, Barthel LK, Raymond PA, Lubensky DK (2012) Coupling mechanical deformations and planar cell polarity to create regular patterns in the zebrafish retina. *PLoS Comput Biol* 8:e1002618.
45. Muto A, et al. (2017) Activation of the hypothalamic feeding centre upon visual prey detection. *Nat Commun* 8:15029.
46. Muto A, Kawakami K (2018) Ablation of a neuronal population using a two-photon laser and its assessment using calcium imaging and behavioral recording in zebrafish larvae. *J Vis Exp* 136:e57485.
47. Asaoka Y, Mano H, Kojima D, Fukada Y (2002) Pineal expression-promoting element (PIPE), a cis-acting element, directs pineal-specific gene expression in zebrafish. *Proc Natl Acad Sci USA* 99:15456–15461.
48. Langmead B, Trapnell C, Pop M, Salzberg SL (2009) Ultrafast and memory-efficient alignment of short DNA sequences to the human genome. *Genome Biol* 10:R25.
49. Zhang Y, et al. (2008) Model-based analysis of ChIP-seq (MACS). *Genome Biol* 9:R137.
50. Workman CT, et al. (2005) enoLOGOS: A versatile web tool for energy normalized sequence logos. *Nucleic Acids Res* 33:W389–W392.